Raman spectral studies of the dynamics of ions in molten LiNO3–RbNO3 mixtures. II. Vibrational dephasing: Roles of fluctuations of coordination number and concentration

ARTICLE *in* THE JOURNAL OF CHEMICAL PHYSICS · MARCH 1986

Impact Factor: 2.95 · DOI: 10.1063/1.450224

1 AUTHOR:

Toshiko Kato
Kyoto Seibo Jogakuin Jr. College
34 PUBLICATIONS **451** CITATIONS

Raman spectral studies of the dynamics of ions in molten $LiNO_3$–$RbNO_3$ mixtures. II. Vibrational dephasing: Roles of fluctuations of coordination number and concentration

Toshiko Katō
Seibo Jogakuin, Jr. College, 1 Taya-cho, Fukakusa, Fushimi-ku, Kyoto 612, Japan

(Received 19 August 1985; accepted 8 October 1985)

The isotropic Raman spectra of the ν_1 (A_1') mode of NO_3^- ions are measured in molten $LiNO_3$–$RbNO_3$ mixtures at various concentrations and at temperatures from 478 to 750 K. The isotropic Raman bandwidth Γ_{iso} is found to increase almost linearly with the mole fraction $c(Li^+)$ of $LiNO_3$, from 9–13 cm^{-1} for molten $RbNO_3$ to 26–27 cm^{-1} for molten $LiNO_3$. Vibrational correlation functions are analyzed on the basis of a model of simultaneous homogeneous and inhomogeneous vibrational dephasing. The contribution of inhomogeneous dephasing was found to be negligibly small in mixtures of $c(Li^+) \lesssim 0.33$. While in mixtures of concentrations $c(Li^+) \gtrsim 0.5$, homogeneous and inhomogeneous processes are found to give comparable contributions to the total vibrational widths, where the latter contribution increases as the temperature decreases. The observed isotropic Raman bands are asymmetric. The asymmetry parameter $\alpha = \Gamma_l/\Gamma_h$, where Γ_l and Γ_h are the half-widths at half-maximum height of the low and high frequency sides of the band, is larger than one in molten $LiNO_3$ and $RbNO_3$, while α is smaller than one in molten mixtures of concentrations $c(Li^+) = 0.33$–0.67. This concentration dependent asymmetry is found to arise predominantly from coordination number fluctuation, i.e., fluctuation of the environmental cation number of a reference NO_3^- ion, while concentration fluctuation in the coordination sphere plays a minor role. A model of local environmental states in a molten mixture, which assumes a linear change of vibrational frequency with neighboring cation numbers, is presented. The observed spectral asymmetry can be interpreted by assuming that the equilibrium distribution has a peak at the small coordination number side in pure molten $LiNO_3$ and $RbNO_3$, while the distribution peak shifts to the high coordination number side in molten mixtures.

I. INTRODUCTION

Isotropic Raman spectra of the ν_1 mode of NO_3^- in a series of molten nitrates, $LiNO_3$, $NaNO_3$, KNO_3, $RbNO_3$, $CsNO_3$, $AgNO_3$, and $TlNO_3$, were measured at a temperature 10–20 K above each melting point, and the vibrational dephasing mechanisms were investigated by Katō and Takenaka.[1] It was found that the isotropic Raman bandwidth Γ_{iso} increases and the vibrational correlation function $G_v(t)$ decays rapidly in the order, $TlNO_3 < RbNO_3 < CsNO_3 \lesssim KNO_3 < NaNO_3$, $AgNO_3 < LiNO_3$, which is almost parallel with the order of decreasing rotational diffusion for molten alkali metal nitrates. Temperature dependence of the Raman spectra in molten $NaNO_3$ at 591–725 K showed that Γ_{iso} increases slightly as the temperature rises. The vibrational correlation functions were analyzed on the basis of a model of simultaneous homogeneous and inhomogeneous vibrational dephasing. It was found that the vibrational frequency modulation is rather fast in molten $RbNO_3$, while homogeneous and inhomogeneous broadening give comparable contributions in strongly interacting molten $LiNO_3$.

In the present paper we study two melts, $LiNO_3$ and $RbNO_3$, which are characterized by the broadest and the sharpest isotropic Raman bands in alkali metal nitrates, respectively, and their mixtures. Vibrational dephasing mechanisms will be studied as a function of concentration and temperature.

The observed isotropic Raman bands were asymmetric. The peak frequency was on the high frequency side of the band center, i.e., $\alpha > 1$, in all molten nitrates investigated in Ref. 1. Two processes for the observed asymmetry were presented. One is an asymmetric distribution of local environmental states with different vibrational frequencies, and another is the contribution of hot bands to the low frequency side of the main band of anharmonic oscillators in the ground state. The observed asymmetric isotropic Raman spectra could be interpreted by either of the two processes. However we could not determine which process was dominant.

In the present molten $LiNO_3$–$RbNO_3$ mixtures, we have observed inverse asymmetry ($\alpha < 1$) in some concentration range. The mechanisms for the observed concentration dependence of the spectral asymmetry will be discussed and a model of local environmental states will be presented in order to interpret qualitatively the observed asymmetry.

Our main objective is to understand the vibrational dephasing mechanisms of asymmetric isotropic Raman bands as a function of mole fraction and temperature. Molten $LiNO_3$–$RbNO_3$ mixtures of various mole fractions, $c(Li^+) = 1.0, 0.8, 0.67, 0.5, 0.33, 0.2, 0.0$ [corresponding mole ratios are $c(Li^+):c(Rb^+) = 1{:}0, 4{:}1, 2{:}1, 1{:}1, 1{:}2, 1{:}4, 0{:}1$, respectively], were investigated in the temperature range from just above the melting point to just below the temperature of decomposition. The experimental procedure and the methods of analysis have been given in part I. Four-

 0021-9606/86/063409-09$02.10

ier transformations were performed by direct numerical integration over 720 points in the frequency range of 360 cm^{-1}. Origin of the frequency was set at the peak frequency of the band.

II. VIBRATIONAL CORRELATION FUNCTIONS

One of the Raman spectra of the ν_1 (A_1') mode of NO_3^- in molten $LiNO_3$–$RbNO_3$ mixtures is shown in Fig. 1. The vibrational correlation functions $G_v(t)$ calculated from the isotropic Raman spectra are shown in Figs. 2–5. Isotropic Raman bandwidth Γ_{iso} is the broadest in molten $LiNO_3$ (26–27 cm^{-1}) and the sharpest in $RbNO_3$ (9–13 cm^{-1}) in a series of molten alkali metal nitrates from $LiNO_3$ to $CsNO_3$.[1] Γ_{iso} of the molten $LiNO_3$–$RbNO_3$ mixtures decreases almost linearly with decreasing $c(Li^+)$ (Table I and Fig. 6). This order of decreasing dephasing rate is identical with the order of increasing rotational mobility of the inertial rotation and rotational diffusion. As large Rb^+ cations are added to molten $LiNO_3$, the vibrational dephasing rate is considered to decrease and the rotational motion is considered to be more rapid because of the small NO_3^-–Rb^+ interaction as compared with the NO_3^-–Li^+ interaction. Concentration dependence of the peak frequency is plotted in Fig. 7.

The band shapes of the isotropic Raman spectra in molten nitrates and in aqueous nitrate solutions have been found to be derived predominantly from pure vibrational dephasing, i.e., changes of the vibrational frequencies due to fluctuations in the molecular environment.[1–4] If these fluctuations can be divided into a fast process ($\Delta\omega_h\tau_h < 1$, where $\Delta\omega_h$ and τ_h are the characteristic width and time of the process), and a very slow process of characteristic width $\Delta\omega_i$ and time τ_i satisfying $\Delta\omega_i\tau_i \gg 1$, the vibrational correlation function will be approximated by the simultaneous homogeneous and inhomogeneous vibrational dephasing model[1,5,6]:

$$G_v(t) = \Phi_{hom}(t)\Phi_{inh}(t), \tag{1}$$

where

$$\Phi_{hom}(t) = \exp\{-\Delta\omega_h^2\,[\tau_h^2(\exp(-t/\tau_h)-1)+\tau_h t\,]\}, \tag{2}$$

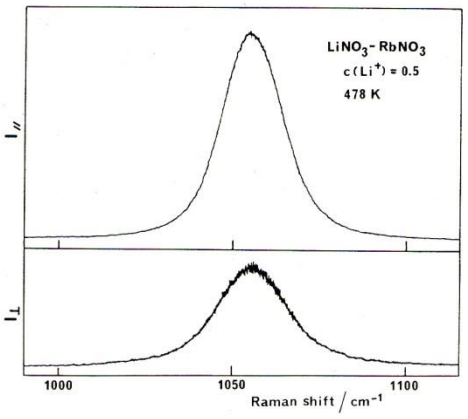

FIG. 1. Polarized and depolarized Raman spectra for the ν_1 (A_1') mode of NO_3^- in a molten $LiNO_3$–$RbNO_3$ mixture of $c(Li^+) = 0.5$ at 478 K. Spectral slit width is 5.28 cm^{-1}. Intensities are in arbitrary units.

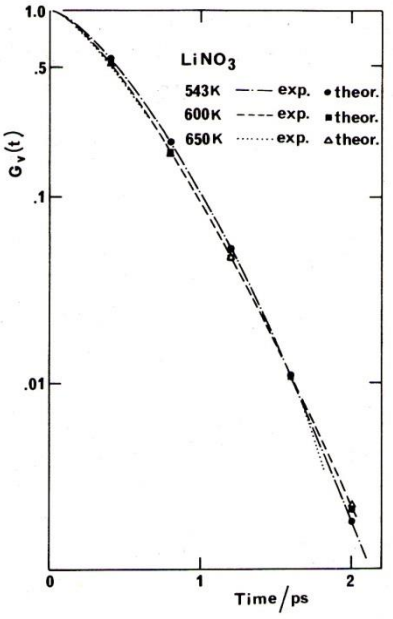

FIG. 2. Vibrational correlation functions for the ν_1 (A_1') mode of NO_3^- in molten $LiNO_3$ at 543, 600, and 650 K. The experimental correlation functions are shown by curves, and fits based on the simultaneous homogeneous and inhomogeneous vibrational dephasing model are shown by points. The optimized parameters are listed in Table II.

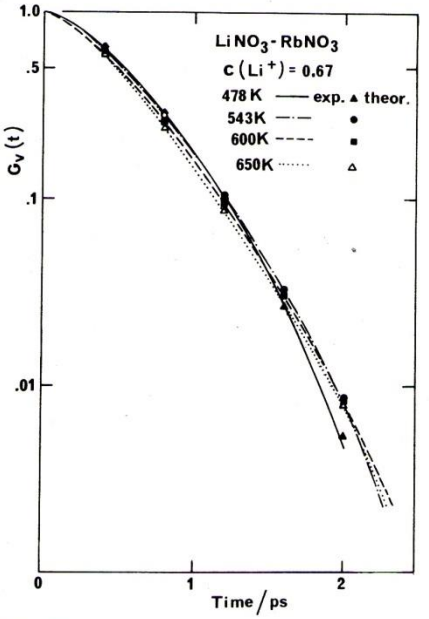

FIG. 3. Vibrational correlation functions for the ν_1 (A_1') mode of NO_3^- in a molten $LiNO_3$–$RbNO_3$ mixture of $c(Li^+) = 0.67$ at 478–650 K. The experimental correlation functions are shown by curves, and fits based on the simultaneous homogeneous and inhomogeneous vibrational dephasing model are shown by points. The optimized parameters are listed in Table II.

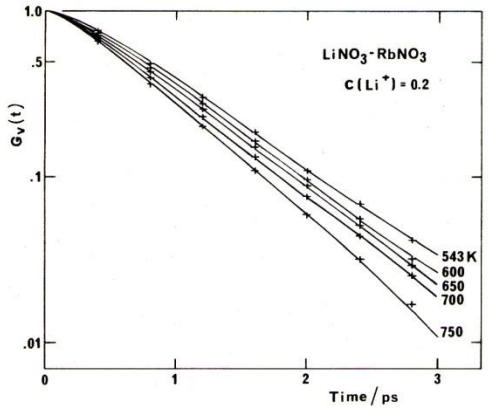

FIG. 4. Vibrational correlation functions for the ν_1 (A_1') mode of NO_3^- in a molten $LiNO_3$–$RbNO_3$ mixture of $c(Li^+) = 0.2$ at 543–750 K. The experimental correlation functions are shown by solid curves, and fits based on the simultaneous homogeneous and inhomogeneous vibrational dephasing model are shown by crosses. The optimized parameters are listed in Table II.

$$\Phi_{\text{inh}}(t) = \exp\{-\tfrac{1}{2}\Delta\omega_i^2 t^2\}. \tag{3}$$

The homogeneous dephasing function, Eq. (2), represents fast dephasing processes such as the fluctuations of the interionic distance and angle in a definite local structure. The inhomogeneous dephasing function, Eq. (3), represents a limiting case of slow modulation ($\Delta\omega_i\tau_i \gg 1$), by which the slow interactions such as the transition between local structures by the diffusion process can be approximated.

The model function defined by Eqs. (1)–(3) was fitted to the experimental $G_v(t)$ by using the experimental vibrational second moment $M_v = \Delta\omega_h^2 + \Delta\omega_i^2$, and by optimizing $\Delta\omega_h^2$ and τ_h by the least squares method.[4,5] The results are listed in Table II, and the theoretical correlation functions corresponding to the parameters are plotted in Figs. 2–5.

TABLE I. Peak frequency, bandwidth, relaxation time, and asymmetry parameter of the isotropic Raman band for the ν_1 (A_1') mode of NO_3^- in molten $LiNO_3$–$RbNO_3$ mixtures.

Concentration $c(Li^+)$	T/K	Peak frequency/ cm^{-1}	Γ_{iso}/cm^{-1}	τ_v/ps	α[a]
1.0	543	1062.6	26.2	0.41	1.16
	600	1059.8	27.2	0.39	1.20
	650	1058.3	26.9	0.39	1.12
0.80	543	1058.6	23.6	0.45	1.04
	600	1056.5	24.2	0.44	1.04
	650	1055.8	24.7	0.43	1.02
0.67	478	1058.0	21.9	0.48	1.00
	543	1056.0	21.6	0.49	1.00
	600	1054.6	22.0	0.48	1.03
	650	1052.8	22.7	0.47	1.00
0.50	478	1055.3	19.0	0.56	0.94
	543	1052.7	19.2	0.55	0.90
	600	1052.0	19.6	0.54	0.92
	650	1050.4	20.0	0.55	0.91
0.33	478	1052.5	14.4	0.74	0.81
	543	1050.7	15.2	0.70	0.85
	600	1049.3	15.8	0.67	0.89
	650	1048.1	16.3	0.65	0.94
	700	1047.0	16.7	0.64	1.00
0.20	543	1048.9	12.3	0.86	0.90
	600	1047.7	12.9	0.82	1.01
	650	1046.5	13.6	0.78	1.10
	700	1045.4	14.3	0.74	1.14
	750	1044.3	14.7	0.68	1.26
0.0	600	1045.6	9.4	1.14	1.31
	650	1045.0	10.6	1.01	1.37
	700	1043.5	11.6	0.92	1.45
	750	1042.3	13.0	0.82	1.49

[a] The effect of the slit width is removed, while it is not removed in deriving α of the Tables 5 and 6 in Ref. 1.

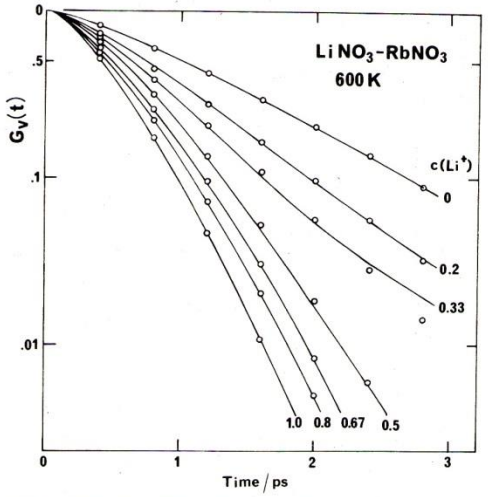

FIG. 5. Vibrational correlation functions for the ν_1 (A_1') mode of NO_3^- in molten $LiNO_3$–$RbNO_3$ mixtures of various concentrations at 600 K. The experimental correlation functions are shown by solid curves, and fits based on the simultaneous homogeneous and inhomogeneous vibrational dephasing model are shown by open circles. The optimized parameters are listed in Table II.

The shape of $G_v(t)$ changes drastically between mixtures of mole fractions $c(Li^+) \lesssim 0.33$ and $c(Li^+) \gtrsim 0.5$ as we see in Fig. 5. In the former mixtures the contribution of inhomogeneous dephasing is negligibly small (Table II), and $G_v(t)$ decays exponentially, i.e., linearly in the semilog scale, at long times as we see in Figs. 4 and 5. Γ_{iso} increases and $G_v(t)$ decays rapidly with increasing temperature in these molten mixtures.

However, in the $LiNO_3$–$RbNO_3$ mixtures of mole fractions $c(Li^+) \gtrsim 0.5$, we find considerable contributions of inhomogeneous broadening (Table II). The $\ln G_v(t) - t$ curve persists its curvature for long times as we see in Figs. 2, 3, and 5. This is understood because the vibrational frequency correlation functions can be calculated from Eqs. (1)–(3) as[5,6]

$$\langle\omega(0)\omega(t)\rangle = -\frac{d^2}{dt^2}\ln G_v(t) = \Delta\omega_h^2 \exp(-t/\tau_h) + \Delta\omega_i^2 \tag{4}$$

which tends to a constant, $\Delta\omega_i^2$, as t increases. The temperature dependence of Γ_{iso} and $G_v(t)$ becomes so small that it is

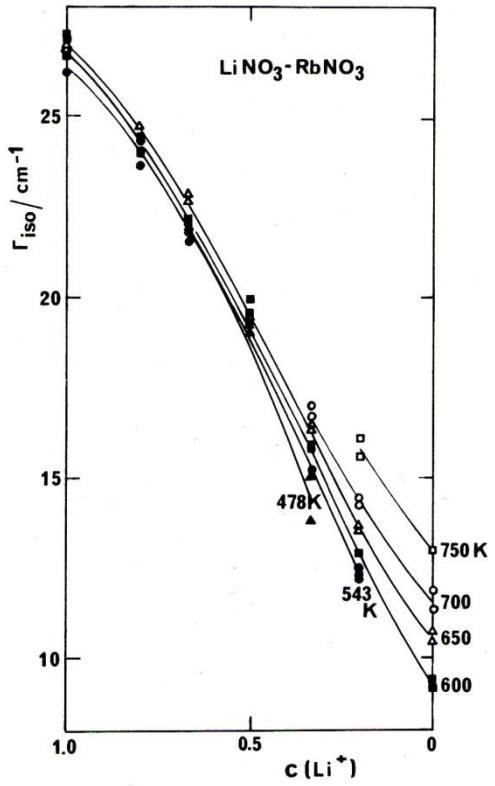

FIG. 6. Concentration and temperature dependence of the isotropic Raman bandwidth of the $\nu_1(A_1')$ mode of NO_3^- in molten $LiNO_3$–$RbNO_3$ mixtures.

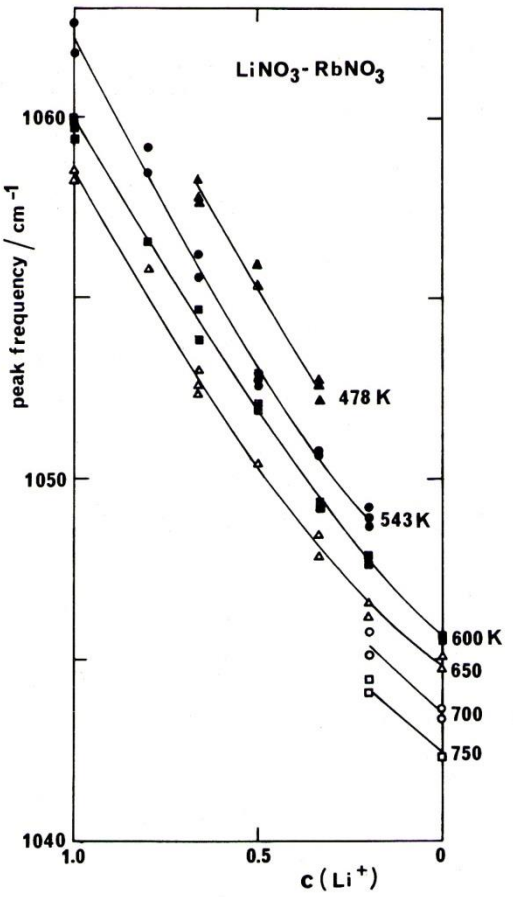

FIG. 7. Concentration and temperature dependence of the peak frequency of the $\nu_1(A_1')$ mode of NO_3^- in molten $LiNO_3$–$RbNO_3$ mixtures.

comparable to the experimental error in the Li^+ rich mixtures (Figs. 2, 3, and 6).

III. ASYMMETRY OF ISOTROPIC RAMAN BAND SHAPES

The isotropic Raman spectra were asymmetric; the peak frequency was on the high frequency side of the band in all molten nitrates investigated in Ref. 1. The extent of asymmetry is characterized by the asymmetry parameter $\alpha = \Gamma_l/\Gamma_h$, where Γ_l and Γ_h are HWHH's measured at the low and high frequency sides of the peak frequency, respectively. Although the model vibrational correlation function, Eqs. (1)–(3), contains fast and slow processes simultaneously, it assumes a symmetric Gaussian distribution of vibrational frequencies for the slow fluctuation [Eq. (3)], and therefore it cannot explain the observed asymmetry of the isotropic Raman spectra.

A. Mechanisms of asymmetry

Spectral asymmetry arises essentially from an asymmetric distribution of vibrational frequencies in a system. Three processes may be proposed for the spectral asymmetry: (a) Asymmetric distribution of local environmental states of oscillators which have linear vibrational frequency dispersion (i.e., constant density of states per unit vibrational frequency difference), which is schematically shown in Fig. 8(a). (b) Symmetric distribution of local environmental states with nonlinear vibrational frequency dispersion (asymmetric density of states per unit vibrational frequency difference) as is schematically shown in Fig. 8(b). (c) The contribution of hot bands to the low frequency side of the main band of anharmonic oscillators in the ground vibrational state,[1] which is found to give the asymmetry of the type $\alpha > 1$.

The concentration and temperature dependence of the asymmetry parameter α of the isotropic Raman band in molten $LiNO_3$–$RbNO_3$ mixtures is plotted in Fig. 9. Spectral asymmetry in pure $LiNO_3$ of the type $\alpha > 1$ decreases with decreasing $c(Li^+)$, and it leads to the inverse asymmetry ($\alpha < 1$) in the concentration range $c(Li^+) = 0.67$–0.33 (see Fig. 1). Then α increases to the largest asymmetry $\alpha = 1.3$–1.5 in molten $RbNO_3$ (Fig. 1 of part I). The inverse asymmetry, $\alpha < 1$, observed in $LiNO_3$–$RbNO_3$ mixtures is opposite to the asymmetry, $\alpha > 1$, expected for the contribution of hot bands from vibrationally excited levels. Here we can conclude that the process (c), the contribution of hot bands, does not play a dominant role in determining the asymmetry of the isotropic Raman bands even in pure $LiNO_3$ and $RbNO_3$, and that the process (a) or (b) will be the dominant process.

TABLE II. Parameters characterizing the homogeneous and inhomogeneous vibrational dephasing processes for the ν_1 (A_1') mode of NO_3^- in molten $LiNO_3$–$RbNO_3$ mixtures. Experimental vibrational widths are also listed.

Concentration $c(Li^+)$	T/K	M_v/cm^{-2}	$\Delta\omega_h^2$/cm^{-2}	τ_h/ps	$\Delta\omega_i^2$/cm^{-2}	Γ_L[a]/cm^{-1}	Γ_G[b]/cm^{-1}	Γ_{iso}/cm^{-1}
1.0	543	400	355	0.133	45	17.8	15.8	26.2
	600	420	390	0.159	30	23.4	12.9	27.2
	650	440	413	0.155	27	24.1	12.2	26.9
0.80	543	360	325	0.136	35	16.7	13.9	23.6
	600	390	364	0.144	26	19.7	12.0	24.2
	650	420	407	0.160	13	24.5	8.5	24.7
0.67	478	290	242	0.113	48	10.3	16.3	21.9
	543	320	290	0.137	30	15.0	12.9	21.6
	600	350	325	0.140	25	17.1	11.8	22.0
	650	370	350	0.149	20	19.6	10.5	22.7
0.50	478	240	205	0.125	35	9.7	10.9	19.0
	543	270	249	0.149	21	14.0	10.8	19.2
	600	290	273	0.160	17	16.5	9.7	19.6
	650	310	302	0.164	8	18.7	6.7	19.4
0.33	478	200	197	0.180	3	13.4	4.1	14.4
	543	220	215	0.174	5	14.1	5.3	15.2
	600	250	244	0.158	6	14.5	5.8	15.8
	650	280	274	0.147	6	15.2	5.8	16.3
	700	310	307	0.146	3	16.9	4.1	16.7
0.20	543	210	208	0.149	2	11.7	3.3	12.3
	600	240	237	0.135	3	12.1	4.1	12.9
	650	270	268	0.128	2	12.9	3.3	13.6
	700	300	300	0.129	0	14.6	0.0	14.3
	750	330	329	0.126	1	15.6	2.4	14.7
0.0	600	130	127	0.168	3	8.0	4.1	9.3
	650	180	177	0.139	3	9.3	4.1	10.6
	700	230	227	0.121	3	10.3	4.1	11.6
	750	290	287	0.105	3	11.4	4.1	13.0

[a] Lorentzian width given by $\Gamma_L = 4\pi c\Delta\omega_h^2\,\tau_h$.
[b] Gaussian width given by $\Gamma_G = 2(2\ln 2)^{1/2}\Delta\omega_i$.

In general the distribution of local environmental states is asymmetric and the vibrational frequency dispersion is nonlinear (i.e., the density of states per unit vibrational frequency difference is not constant), and both effects will contribute to asymmetry in some cases and cancel in other cases. Because the explanation of asymmetric Raman bands by the process (b) will lead to an unrealistic vibrational frequency dispersion in molten mixtures as will be discussed later, we shall now discuss the effect of asymmetric distribution of local environmental states with linear vibrational frequency dispersion.

B. Coordination number fluctuation in pure molten nitrates: the MKF model

The asymmetric isotropic Raman band shapes of molten $LiNO_3$ and $RbNO_3$ have been analyzed by an analytical model of the static and dynamical fluctuation of cation numbers surrounding a reference NO_3^- ion.[1] Let us outline the model first, which will be extended to binary molten mixtures in the next section. A model of local environmental states for neat liquids by Knapp and Fischer[7] was modified so that it could be applied to molten nitrates, which we will call the MKF model.[1]

X-ray and neutron diffraction experiments[8,9] and molecular dynamics simulation (MD) combined with them[10] show that the NO_3^- ions in ionic melts are most probably surrounded by cations. In the MKF model, local environmental states of NO_3^- ions are classified into $N+1$ states with $n = a, a+1, \ldots, a+N$ perturber cations which are in contact with the reference anion. Here we shall call the number of cations surrounding an NO_3^- ion as coordination number. The transition between these environmental states due to diffusion processes is assumed to be a Markovian process. The perturber cations are assumed to act independently and equivalently, and each perturber induces a discrete shift $\Delta\omega$ of the vibrational frequency. This corresponds to the linear change of vibrational frequency with coordination number n. The modulation of each perturber is assumed to be switched on with rate R and off rate kR. If the equilibrium distribution probability of $N+1$ environmental states is represented by a $N+1$ dimensional vector $P^e = (p_a^e, p_{a+1}^e, \ldots, p_{a+N}^e)$, where $\Sigma_{n=a}^{a+N} p_n^e = 1$, and if the vibrational frequency modulation is slow, $\Delta\omega \gg R$, the spectrum is expressed as a superposition of component lines for all environmental states,

$$I(\omega) = \sum_{n=a}^{a+N} p_n^e f_n(\omega - \omega_0 - n\Delta\omega). \tag{5}$$

The equilibrium distribution of environmental states of NO_3^- ions, which has a peak at the small coordination number side, has been proposed by the MD simulations of molten

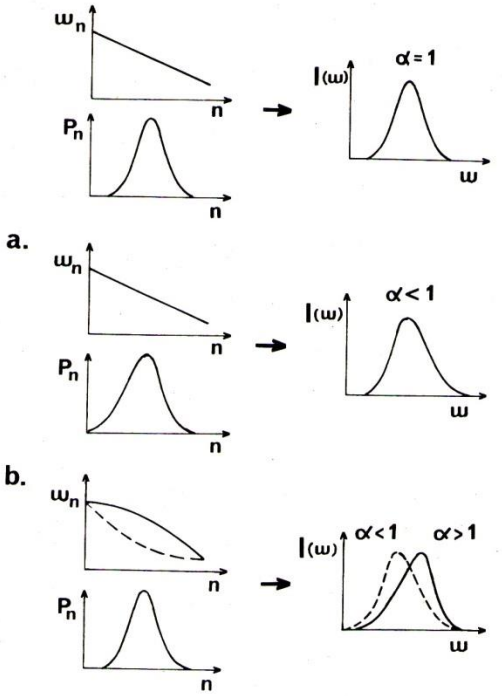

FIG. 8. Mechanisms of asymmetric isotropic Raman bands. Top: Symmetric distribution of local environmental states, characterized by n, which has a linear vibrational frequency dispersion, gives rise to a symmetric isotropic Raman band. (a): Asymmetric distribution of local environmental states which has a linear vibrational frequency dispersion gives rise to an asymmetric band. (b): Symmetric distribution of local environment states which has a nonlinear vibrational frequency dispersion gives rise to an asymmetric band.

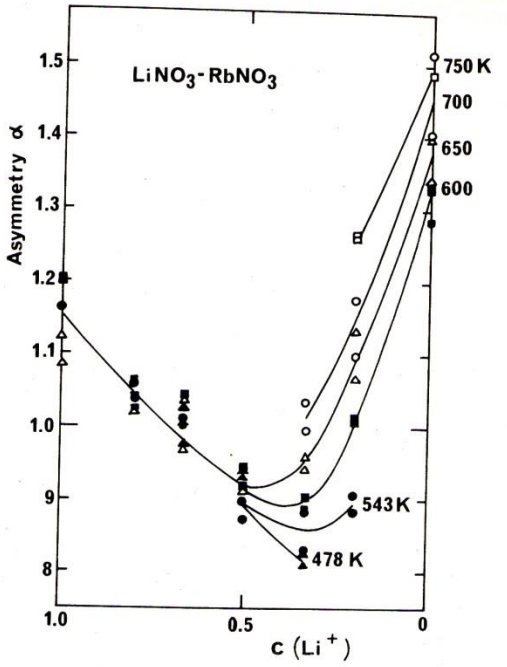

FIG. 9. Concentration and temperature dependence of the asymmetry parameter $\alpha = \Gamma_l/\Gamma_h$ of isotropic Raman bands in molten $LiNO_3$–$RbNO_3$ mixtures.

$LiNO_3$ and $RbNO_3$ combined with the x-ray and neutron diffraction data.[1,10] Coordination numbers were distributed in the range $n = 4,5,6,7,8$ ($a = 4$, $N = 4$) for molten $LiNO_3$ and $n = 5,6,7,8,9$ ($a = 5$, $N = 4$) for molten $RbNO_3$. Therefore, if we assume a red shift ($\Delta\omega < 0$) upon increasing coordination number n and that the shapes of the component lines are all the same, the spectrum will have the asymmetry of the type $\alpha > 1$, which is coincident with the asymmetry observed in all molten nitrates studied in Ref. 1.

We tried to fit two spectra, one is for the equilibrium distribution P^e obtained by the MD simulations,[1,10] and the other is for the P^e calculated on the basis of the MKF model, to the observed spectra of molten $LiNO_3$ and $RbNO_3$.[1] By adjusting $\Delta\omega$ and k values, the model calculation could reproduce the observed isotropic Raman spectra of molten $LiNO_3$ fairly well, but could not reproduce the observed highly asymmetric spectrum of molten $RbNO_3$ within experimental error. Parameters which give the best fit to the experimental spectra are listed in Table III.

C. Coordination number fluctuation and concentration fluctuation in molten nitrate mixtures

In order to explore the concentration dependence of isotropic Raman band shapes of NO_3^- ions in molten $LiNO_3$–$RbNO_3$ mixtures, we have to extend the model of local environmental states for pure melts to be applicable to molten salt mixtures. We find that the total shift of the peak frequency of the isotropic Raman band between molten $LiNO_3$ and $RbNO_3$ is $\Delta\Omega = -14.2\ \mathrm{cm}^{-1}$ at 600 K and $-13.3\ \mathrm{cm}^{-1}$ at 650 K (Table I and Fig. 7), and the total change of Γ_{iso} is $\Delta\Gamma = -17.8\ \mathrm{cm}^{-1}$ at 600 K and $-16.3\ \mathrm{cm}^{-1}$ at 650 K (Table I and Fig. 6). Because $|\Delta\Gamma| \cong 17\ \mathrm{cm}^{-1}$ is larger than $|\Delta\Omega| \cong 14\ \mathrm{cm}^{-1}$ in molten $LiNO_3$–$RbNO_3$ mixtures, we have to consider the coordination number fluctuation and concentration fluctuation in the coordination sphere of a nitrate ion simultaneously, in which the former plays a more important role. We have just presented an outline of the model of the number fluctuation of cations surrounding an NO_3^- ion in pure molten nitrates. An analytical model for the static and dynamical concentration fluctuation at the reference molecule in liquid binary mixtures has been proposed by Knapp and Fischer.[11]

Let us combine them and construct a unified model of vibrational states in molten nitrate mixtures. We classify the environmental states of an anion by a point (m,n) in the two-dimensional space of the number of Li^+ ions m along the OX axis, and the number of Rb^+ ions n along the OY axis, which are in contact with the reference anion (Fig. 10). We have to determine both the vibrational frequency dispersion $\omega(m,n)$ and the equilibrium distribution probability $P^e = \{p^e_{mn}\}$ as functions of the state (m,n). In the spectral study of pure $LiNO_3$ and $RbNO_3$ melts,[1] we have assumed a linear vibrational frequency dispersion which decreases ($\Delta\omega < 0$) with

TABLE III. Results of analysis of the asymmetric isotropic Raman band ν_1 (A_1') in pure molten nitrates, based on the model of discrete environmental states of NO_3^- surrounded by n cations, with vibrational frequencies $\omega_0 + n\Delta\omega$. The equilibrium distribution P^e was calculated by the MKF model[1] and by the MD simulations.[1,10]

System	T/K	Component line $\Delta\omega_h^2$/cm^{-2}	τ_h/ps	Model	$\Delta\omega$/cm^{-1}	k	P^e/%	Γ^{th}/cm^{-1}	α^{th}	Γ^{exp}/cm^{-1}	α^{exp} [a]
							$n = 4,5,6,7,8$				
$LiNO_3$	543	355	0.133	MKF	−6.2	0.65	(27,34,26,11,2)	26.3	1.14	26.1	1.16
				MD	−7.7		(11,40,36,11,2)	26.5	1.07	26.1	1.16
	600	390	0.159	MKF	−6.2	1.0	(43,34,17,5,1)	27.3	1.15	27.2	1.20
				MD	−6.2		(10,40,36,11,2)	27.3	1.04	27.2	1.20
							$n = 5,6,7,8,9$				
$RbNO_3$	600	127	0.168	MKF	−2.2	0.8	(41,34,18,6,1)	9.8	1.11	9.4	1.31
				MD	−2.2		(10,50,31,7,2)	9.4	1.04	9.4	1.31

[a] The effect of the slit width is removed, while it is not removed in deriving α of the Tables 5 and 6 in Ref. 1.

increasing cation number m or n along the OX or OY axis, and an asymmetric distribution of coordination numbers which has peaks at the small m and n sides. The states corresponding to the peak distribution along the OX and OY axes are represented by $S(5,0)$ and $T(0,6)$,[1] respectively (Fig. 10). As the salt concentration $c(Li^+)$ decreases from 1.0 to 0.0, the point of the peak distribution will change along some curve from S to T.

Because the vibrational frequency changes almost linearly with the concentration $c(Li^+)$ as shown in Fig. 7, we may assume a linear change of the vibrational frequency with the microscopic concentration, i.e., with m, keeping the coordination number $M = m + n$ constant. Assuming that the vibrational frequency of the ν_1 mode of NO_3^- changes linearly with cation numbers m and n along the OX and OY axes, respectively, and with m along the line M = constant, we obtain a vibrational frequency as a function of (m,n) as follows:

$$\omega(m,n) = \frac{m\omega_{Li} + n\omega_{Rb}}{M} + \frac{m(M-5)\Delta\omega_{Li} + n(M-6)\Delta\omega_{Rb}}{M}. \quad (6)$$

This equation gives a frequency dispersion for the molten $LiNO_3$;

$$\omega(m,0) = \omega_{Li} + (m-5)\Delta\omega_{Li}, \quad (7)$$

and for the molten $RbNO_3$;

$$\omega(0,n) = \omega_{Rb} + (n-6)\Delta\omega_{Rb}. \quad (8)$$

Here ω_{Li} is the vibrational frequency of NO_3^- ions in an environmental state (5,0), which corresponds to the maximum distribution in molten $LiNO_3$, and $\Delta\omega_{Li}$ is the vibrational frequency shift upon addition of one Li^+ ion as a neighbor of an NO_3^- ion ($m \to m+1$). ω_{Rb} and $\Delta\omega_{Rb}$ are those for molten $RbNO_3$. The vibrational frequency dispersion $\omega(m,n)$ according to Eqs. (6)–(8) is schematically shown in Fig. 10. The frequency shift corresponding to an interchange of a Li^+ ion in the coordination sphere of a reference NO_3^- ion with a Rb^+ ion outside the sphere can be obtained from Eq. (6) as a function of coordination number;

$$\Delta\omega(M) = \omega(m-1,n+1) - \omega(m,n) = \Delta\omega_{Rb} - \Delta\omega_{Li} + \frac{1}{M}\{\omega_{Rb} - \omega_{Li} + 5\Delta\omega_{Li} - 6\Delta\omega_{Rb}\}. \quad (9)$$

From the analysis of the asymmetric isotropic Raman band

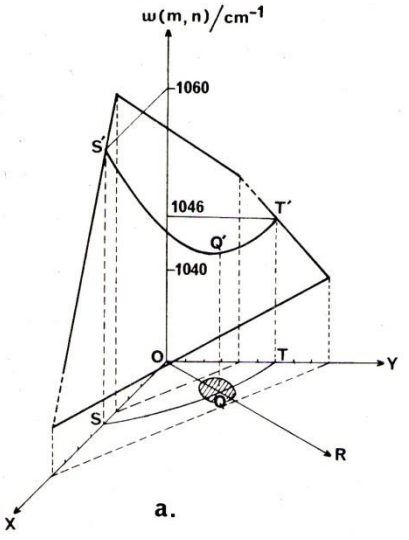

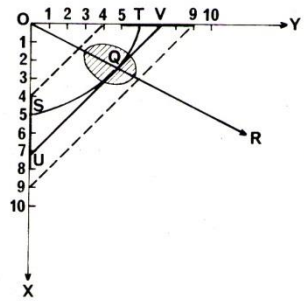

FIG. 10. A vibrational frequency dispersion $\omega(m,n)$ as a function of local environmental state (m,n) of an NO_3^- ion in molten $LiNO_3$–$RbNO_3$ mixtures. The line OR shows the composition of a mixture, and the point of the peak distribution changes along a curve ST, where $S(5,0)$ and $T(0,6)$. The distribution of local states is confined to a range (shaded part) surrounding a point of intersection Q of the curve ST and the line OR. UV is the line of constant cation number passing Q.

shapes in pure molten nitrates based on the model of discrete environmental states,[1] we have estimated the values of the parameters. They are $\omega_{Li} = 1060\ cm^{-1}$, $\omega_{Rb} = 1046\ cm^{-1}$, $\Delta\omega_{Li} = -6.2\ cm^{-1}$, $\Delta\omega_{Rb} = -2.2\ cm^{-1}$, at 600 K (Tables I and III). By substituting these values in Eq. (9), $\Delta\omega(M)$ is calculated to be $\Delta\omega(4) = -4.0\ cm^{-1}$, $\Delta\omega(5) = -2.4\ cm^{-1}$, $\Delta\omega(6) = -1.3\ cm^{-1}$, $\Delta\omega(7) = -0.6\ cm^{-1}$, $\Delta\omega(8) = 0\ cm^{-1}$, $\Delta\omega(9) = 0.4\ cm^{-1}$ at 600 K, which shows negative gradient of the vibrational frequency with decreasing m for $M = 4, 5, 6$, while $\Delta\omega(M) \doteqdot 0$ for $M = 7, 8, 9$.

If we assume almost linear vibrational frequency dispersion of the environmental states as in Eq. (6), the asymmetric band will be ascribed only to an asymmetric distribution of local environmental states. Let us take an example of a mixture of $c(Li^+) = 0.33$. In Fig. 10 the line *OR* shows this composition $[c(Li^+):c(Rb^+) = 1:2]$. The distribution of local states will be confined to a range (shaded part) which surround a point of intersection Q of the curve *ST* and the line *OR*. If the point of the peak distribution deviates from the center of the distribution range, the band will be asymmetric. *UV* is the line of constant coordination number (M = constant) passing Q.

Let us see the three-dimensional surface of the distribution probability, p^e_{mn}, from the cross section of the surface along the *OR* (coordination number fluctuation) and the *UV* (concentration fluctuation) axes. The concentration dependent distribution probabilities of the local states along the *UV* and *OR* axes are shown in Fig. 11. In an equimolar mixture of $c(Li^+) = 0.5$, the distribution along the *UV* axis will be symmetric. The process which can explain the asymmetry $\alpha < 1$ in an equimolar mixture should be sought in the distribution along the *OR* axis. In pure molten nitrates the peak distribution was at the low coordination number side of the total distribution which gave the spectral asymmetry of the type $\alpha > 1$. However, in order to explain the asymmetry of the type $\alpha < 1$ in an equimolar mixture, we must assume that the point of the peak distribution shifts to the high M side of the total distribution along the *OR* axis. Therefore we propose a model that the point corresponding to the peak distribution changes not along the straight line *ST* but along a curve *ST* which deviates to the high M side of the line *ST*.

From the above discussions and from the data of $|\Delta\Gamma| > |\Delta\Omega|$, we conclude that the coordination number fluctuation along the *OR* axis is the dominant mechanism for determining the asymmetric band profiles, and the concentration fluctuation in the coordination sphere along the *UV* axis plays a minor role. The contributions of the local state distributions along the *UV* axis [Fig. 11(a)] and the *OR* axis [Fig. 11(b)] to the asymmetry parameter α are shown schematically in Figs. 12(a) and 12(b), respectively, as functions of concentration. The experimental asymmetry parameter α shown in Fig. 9 decreases slowly with decreasing $c(Li^+)$ in the range $c(Li^+) \gtrsim 0.5$, becomes minimum at $c(Li^+) < 0.5$, and increases rapidly at $c(Li^+)$ approaches 0. These characters can be understood quite reasonably as a weighted sum of the contributions from the coordination number fluctuation along the *OR* axis and the concentration fluctuation along the *UV* axis as shown in Fig. 12(c).

According to this model, the peak vibrational frequency will decrease along the curve $S'Q'T'$ in Fig. 10(a). The peak frequency will decrease rapidly in the range $c(Li^+) > 0.5$, and slowly in the range $c(Li^+) < 0.5$. This result accords quite well with the characteristic behavior of the almost linear change of the peak vibrational frequency vs concentration shown in Fig. 7.

If we want to explain the observed asymmetry in molten nitrate mixtures by the process (b) in Sec. III A, we have to assume different types of vibrational frequency dispersion vs coordination number. The vibrational frequency dispersion should be of the type shown by a solid curve in Fig. 7(b) along the *OX* and *OY* axes (pure nitrates), and of the type shown by a broken curve along the *OR* axis in molten nitrate mixtures of $c(Li^+) = 0.67$–0.33. There is no reasonable explanation for this change of vibrational frequency dispersion between pure and mixed molten nitrates.

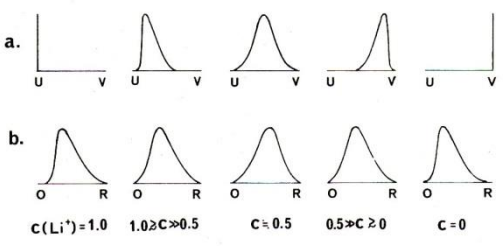

FIG. 11. Cross section of the equilibrium distribution probability of local environmental states (a) along the *UV* axis (concentration fluctuation) and (b) along the *OR* axis (coordination number fluctuation) as a function of concentration of $LiNO_3$–$RbNO_3$ mixtures.

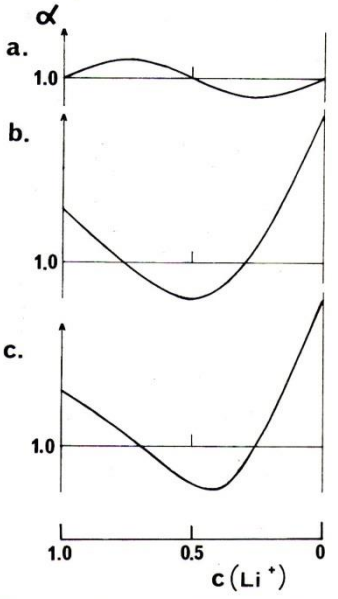

FIG. 12. (a) Contribution of the distribution of environmental states along the *UV* axis to the asymmetry parameter α is shown schematically as a function of concentration. (b) Contribution of the distribution of environmental states along the *OR* axis to the asymmetry parameter α. (c) Concentration dependence of α as a weighted sum of the contributions (a) and (b).

The conclusions of this paper can be summarized as follows. Isotropic Raman bandwidths were found to increase almost linearly with increasing $c(Li^+)$. The contribution of inhomogeneous dephasing was found to be negligibly small in mixtures of concentrations $c(Li^+) \lesssim 0.33$, while in mixtures of concentrations $c(Li^+) \gtrsim 0.5$, homogeneous and inhomogeneous processes give comparable contributions to the total vibrational width, where the latter contribution becomes large as the temperature decreases. It should be noted that the analysis of a real vibrational correlation function, which is a Fourier transformation of an average of the high and low frequency sides of the spectrum [i.e., if the imaginary part of $G_v(t)$ is neglected], will lead to underestimation of the inhomogeneous vibrational dephasing.

Asymmetry of isotropic Raman band profiles in molten nitrates and their mixtures is caused predominantly by the coordination number fluctuation of a reference NO_3^- ion, while concentration fluctuation in the coordination sphere plays a minor role. The change of the asymmetry parameter α can be understood by assuming an almost linear change of

inhomogeneous dephasing was found to be negligibly small in mixtures of concentrations $c(Li^+) \lesssim 0.33$, while in mixtures of concentrations $c(Li^+) \gtrsim 0.5$, homogeneous and inhomogeneous processes give comparable contributions to the total vibrational width, where the latter contribution becomes large as the temperature decreases. It should be noted that the analysis of a real vibrational correlation function, which is a Fourier transformation of an average of the high and low frequency sides of the spectrum [i.e., if the imaginary part of $G_v(t)$ is neglected], will lead to underestimation of the inhomogeneous vibrational dephasing.

Asymmetry of isotropic Raman band profiles in molten nitrates and their mixtures is caused predominantly by the coordination number fluctuation of a reference NO_3^- ion, while concentration fluctuation in the coordination sphere plays a minor role. The change of the asymmetry parameter α can be understood by assuming an almost linear change of

the vibrational frequency with environmental cation numbers, m and n, and an asymmetric distribution of these local environmental states. By assuming a linear vibrational frequency dispersion which decreases ($\Delta\omega < 0$) with increasing coordination number, the distribution is found to have a peak at the small coordination number side in pure molten $LiNO_3$ and $RbNO_3$ which gives the asymmetry $\alpha > 1$, while in molten mixtures the distribution peak shifts to the high coordination number side which gives the asymmetry $\alpha < 1$. In a possible case that the equilibrium distribution in pure melts has a peak at the high coordination number side, the asymmetric spectrum of the type $\alpha > 1$ can be interpreted by assuming a blue shift ($\Delta\omega > 0$) upon increasing coordination number.

[1]T. Katō and T. Takenaka, Mol. Phys. **54**, 1393 (1985).
[2]T. Katō J. Umemura, and T. Takenaka, Mol. Phys. **36**, 621 (1978).
[3]T. Katō and T. Takenaka, Chem. Phys. Lett. **62**, 77 (1979).
[4]T. Katō, Mol. Phys. **39**, 559 (1980).
[5]T. Katō, Mol. Phys. **48**, 1119 (1983).
[6]T. Katō, J. Chem. Phys. **79**, 2139 (1983).
[7]E. W. Knapp and S. F. Fischer, J. Chem. Phys. **74**, 89 (1981).
[8]H. Ohno and K. Furukawa, J. Chem. Soc. Faraday Trans. 1 **74**, 297 (1978).
[9]K. Suzuki and Y. Fukushima, Z. Naturforsch. Teil. A **32**, 1438 (1977).
[10]M. Mikami, I. Okada, T. Yamaguchi, H. Ohtaki, and K. Kawamura, in Proceedings of the 1st International Symposium on Molten Salt Chemistry and Technology, Kyoto, 1983, p. 350.
[11]E. W. Knapp and S. F. Fischer, J. Chem. Phys. **76**, 4730 (1982).